

Flow characteristics of polar liquids in microfluidic immunosensors

Ramchander Chepyala · Siddhartha Panda

Received: 24 April 2013 / Accepted: 19 August 2013 / Published online: 29 August 2013
© Springer-Verlag Berlin Heidelberg 2013

Abstract There is an interest in microfluidic devices for disease detection. In microfluidic immunosensors, the microchannel surfaces are functionalized with a stack of intermediate linker molecules to the specific antibodies. The efficiency of these immunosensors depends on the effective capture of antigens flowing in the carrier fluid by the surface-immobilized antibodies. The diffusion of these antigens to these antibody-immobilized surfaces is governed by the velocity profile, which in turn is governed by the interaction of the carrier fluid molecules with the surface antibodies. We report a systematic study to characterize fluid flow of different polar liquids (water, methanol and isopropyl alcohol) in trapezoidal Si microchannels, of about 100 μm hydraulic diameter, functionalized with intermediate molecular layers along with three different antibodies immobilized via these molecular layers. The friction constants were calculated from the pressure drop measurements. We attempted to understand the solid–liquid interactions in terms of the friction constants as a function of the solid surface free energies of the terminal antibody layers (which are affected by the energetics of the underlying layers) immobilized on to the microchannels, and the polarities of the liquids flowing through these microchannels. Correlations of liquid polarities with the friction constants were seen for almost all the functionalized surfaces. A reasonable correlation of the surface energies with the friction constants was seen for most of the surfaces studied. Possible reasons for the behaviors are discussed. The measured friction constants and the knowledge of the solid–liquid interactions could facilitate improved designs of microfluidic immunosensors.

Keywords Microfluidic immunosensor · Silicon · Antibody · Silane · Surface free energy · Friction

1 Introduction

There is a growing interest in the utilization of microfluidic devices for early disease detection in point-of-care diagnostics (Gubala et al. 2012). In microfluidic immunosensors, the microchannel surfaces are functionalized with a stack of intermediate linker molecules to the specific antibodies, and the flow rates of the liquid samples containing the antigens through the microchannels are usually small (with Reynolds numbers ~ 1). The effectiveness of the sensor depends on the effective capture of antigens by the surface-immobilized antibodies; and the diffusion of the antigens to these antibody-immobilized sensor surfaces is governed by the velocity profile (Cottin-Bizonne et al. 2004; Zimmermann et al. 2005), which in turn is governed by the interaction of carrier fluid molecules with the antibodies on the surfaces. The interactions of these terminal biomolecules at the solid–liquid interface with the fluid molecules are in general dependent on factors such as surface topography, hydrophilicity/hydrophobicity, surface chemistry, and surface charge (Chang and Wang 2011; Andrade et al. 1992; Keselowsky et al. 2004; Mrksich and Whitesides 1996; Brash 1987). There is a large body of work on the interaction of flowing fluid molecules with surfaces immobilized with non-biomolecules (Tretheway and Meinhart 2002; Chao and Fu-Quan 2011; Choi et al. 2003; Nayak et al. 2007) with reported effects of some of the factors mentioned above and the effects of other factors such as microchannel geometry and the nature of the fluids (e.g., polar, ionic). However, to the best of our knowledge, there is very scant work on the same for surfaces

R. Chepyala · S. Panda (✉)
Department of Chemical Engineering, Indian Institute of Technology Kanpur, Kanpur, UP 208016, India
e-mail: spanda@iitk.ac.in

immobilized with biomolecules. Flow studies conducted in microchannels, mostly with non-biofunctionalized surfaces, have focused on heat transfer (García-Hernando et al. 2009; Kandlikar 2012), bulk reaction (Kockmann et al. 2006; Greenway et al. 2000; Watts and Haswell 2005), and mixing applications (Aubin et al. 2010; Lee et al. 2011; Capretto et al. 2011). In case of biofunctionalized surfaces for non-immunosensing applications, most of the studies have focused on improving the biological assay (Salieb-Beugelaar et al. 2010; Miller and Wheeler 2008; Chen et al. 2007), biomolecule patterning techniques on the substrates (Bernard et al. 2000; Falconnet et al. 2006; Lina and Lin 2011), and enhancing the biofunctionalization on surfaces by physical and chemical modification (Jung et al. 2001). Specifically for immunosensing applications, most of the studies have focused on studying the non-flow characteristics (i.e., typically reactions) such as detection of different biomarkers (Zhang et al. 2013; Malhotra et al. 2012; Hu et al. 2010), and dynamics of the antigen and antibody interactions (Gao and Jin 2005). However, for immunosensing applications, we have found no work on the effect of surface-immobilized biomolecules on the fluid flow characteristics. Though studying the immunosensing reactions is important, complete understanding of the flow characteristics of the fluids is needed to improve the reaction kinetics and the designs of microfluidic immunosensors. Therefore, a fundamental understanding of the interaction of the biofunctionalized surfaces with fluids of different natures is important in characterizing the fluid flow.

Of the several major factors stated above which govern the fluid flow in microfluidic channels of non-biofunctionalized surfaces, the surface topography/roughness (Li and Mala 1999; Pfund et al. 2000; Stroock et al. 2002; Hu et al. 2003; Kleinstreuer and Koo 2004; Kandlikar et al. 2005; Celata et al. 2006; Bahrami et al. 2006; Gamrat et al. 2008; Xiong and Chung 2010; Zhou and Yao 2011; Wu and Cheng 2003a; Weilin et al. 2000) and channel geometry (Papautsky et al. 1999a; Gan et al. 2007; Wu and Cheng 2003b; Bahrami et al. 2007; Koo and Kleinstreuer 2004; Morini 2004) have been well studied, while the effects of chemically coated surfaces in conjunction with polar and ionic fluids need further investigation as inconsistencies are reported, and more specifically as there is scant work for biofunctionalized surfaces. The effects of the chemical nature of the surfaces on the fluid flow have been studied by modifying the microchannels with different chemicals such as silanes where reduction in drag, i.e., fluid friction (Chao and Fu-Quan 2011) has been reported to be attributed to fluid slip (Trettheway and Meinhart 2002; Hsieh and Lin 2009; Choi et al. 2003); and it is known that

the different functionalized surfaces (with different functional groups in different orientations) will have different surface free energies and hence will have different interactions with the flowing liquids of different polarities (Cappelletti et al. 2013). The effect of polarity of liquids flowing in the microchannels with non-biofunctionalized surfaces is still not clear where some reports have shown an effect of liquid polarity on the friction factor (Brutin and Tadrist 2003; Brutin et al. 2003; Kulinsky et al. 1999; Papautsky et al. 1999b), the fluid slip (Ulmanella and Ho 2008), and the mass flow rate (Kulinsky et al. 1999; Pfahler et al. 1990), while other reports have not (Judy et al. 2002; Sharp and Adrian 2004).

The subject of the current work is on characterizing the flow of polar liquids in biofunctionalized (antibody immobilized) microchannel surfaces for immunosensing applications. To the best of our knowledge, we are not aware of any such work in the literature. In a previous work (Chepyala and Panda 2013), we studied the surface energetics of three different antibodies (anti-BSA, anti-PSA, and anti-CRP) immobilized on to Si via intermediate functionalized stages, by using one of the three amino-silanes (APTES, TMSPEDA, and TMSPDETA) of different chain lengths and found that the terminal groups and the molecular orientations affected the surface free energies. It is of interest to understand the factors which affect the interaction of terminal antibody layers immobilized inside the microchannels with the liquids of different properties flowing through it. Since the terminal antibody layers are affected by the nature of the stacks of their underlying layers and hence the surface free energies, understanding their interaction with liquids of different properties would help find suitable functional layers in each stack so as to better tune of the properties of the terminal antibody layers. We report a systematic study to characterize fluid flow of different polar liquids (water, methanol, and isopropyl alcohol) in trapezoidal Si microchannels functionalized with intermediate molecular layers (hydroxyl, three different chain lengths of amino-silanes) along with three different antibodies immobilized via these molecular layers. The friction factors were calculated from the pressure drop measurements. We attempted to understand the solid–liquid interactions in terms of the friction factor as a function of the solid surface free energies of the terminal antibody layers (which are affected by the energetics of the underlying layers) immobilized on to the microchannels, and the polarities of the liquids flowing through these microchannels. The measured friction factors and the knowledge of the solid–liquid interactions could facilitate improved designs of microfluidic immunosensors.

2 Materials and methods

2.1 Materials

We have used the same materials as used in our previous work (Chepyala and Panda 2013), and for the sake of completeness, we are mentioning these here. Silicon wafers of $\langle 100 \rangle$ orientation, p-type, with resistivity of 1–20 Ωcm were obtained from Wafer World, USA, and Pyrex glass sheets from Scientific Technologies, India. Ammonia solution 25 %, hydrochloric acid 37 %, sulfuric acid 98 %, hydrogen peroxide 30 %, toluene 99 %, methanol 99 %, and isopropyl alcohol (IPA) 99 % were obtained from Qualigens Fine Chemicals, India; absolute ethanol 99.9 % obtained from S.D. Fine-Chem Ltd., India; 3-aminopropyltriethoxysilane (APTES) 99 %, *N*-[3-(trimethoxysilyl)propyl] ethylenediamine (97 %) (TMSPEDA), *N*1-(3-trimethoxysilylpropyl) diethylenetriamine (97 %) (TMSPDETA) and PBS buffer (pH-7.4) were supplied by Sigma-Aldrich Inc., Germany; glutaraldehyde 25 % obtained from Loba Chemie, India; anti-BSA IgG from Chromous Biotech, India; anti-PSA IgG and anti-CRP IgG from GeneTech Laboratories, India; de-ionized (DI) water (0–0.5 S/m) obtained from Glen RO⁺ Systems and zero-grade nitrogen from Sigma Gases & Services, India; Teflon tubes and connectors from PCI Analytics Pvt. Ltd., India; regulated DC Power supply from APLAB Ltd., India; rechargeable RELICELL battery from Greenvision Technologies Pvt. Ltd., India; and differential pressure transducers from Omega Engineering Inc., USA, syringe pump (PHD 2000 ULTRA) from Harvard Apparatus, USA; DAQ system (NI-9205, NI-9211) from National Instruments, USA.

2.2 Microchannel unit fabrication

2.2.1 Anisotropic etching of microchannels

SiO₂ of thickness approximately 300 nm was grown on as received Si wafers by dry oxidation. These wafers were cut into sizes of 15 mm \times 35 mm and were cleaned by ultrasonication for 2 min followed by the RCA1 and RCA2 cleaning methods at 75 ± 5 °C for 20 min each with subsequent DI water rinsing and drying with N₂ gas. These Si samples were patterned by using a photolithography method, in which a positive photoresist (AZ1500) was spin coated on to the samples at 3,000 rpm for 1 min followed by prebaking at 105 °C for 75 s. These samples were exposed under UV light (360 nm) for 2 min by placing a copper mask of required dimensions on them and then developed in TMAH solution for 1 min followed by postbaking at 105 °C for 90 s. The exposed patterned oxide on the Si samples was etched for 5 min by using BHF

(NH₄F:HF:H₂O in 114:170:28) at 25 °C in a custom-made etching bath specially designed to avoid backside etching. After oxide etching, the samples were dipped in acetone for 1 min to remove the surplus photoresist. Then, anisotropic etching of these Si samples by using 30 % KOH recipe (KOH:H₂O:IPA; 170:190:40) at 80 °C was carried for required time which resulted in microchannels with trapezoidal cross section. Likewise, two samples were anisotropically etched by varying the widths and depths to fabricate microchannels of different hydraulic diameters (about 100 and 65 μm).

2.2.2 Anodic bonding

The Si microchannels were sealed by anodically bonding the Pyrex glass pieces by using a wafer bonder (AML AWB aligner, Applied Microengineering Ltd., UK) at 500 °C after micromachining the through holes of 3 mm in diameter in the plenums using a laser machine (ViolinoTM 3, LASERVALL S.P.A, Italy).

2.2.3 Microfluidic setup

For carrying out the pressure drop experiments through the microchannels, a microfluidic experimental setup, the schematic of which is shown in Fig. 1, was used with a custom made microchannel holder assembly fabricated with Teflon. It contains ports for liquid inlet and outlet, along with the ports each at the upstream and downstream of the sample holder, providing access for in situ measurement of the pressure drop and the liquid temperature. The bonded microchannel was placed on top of the sample

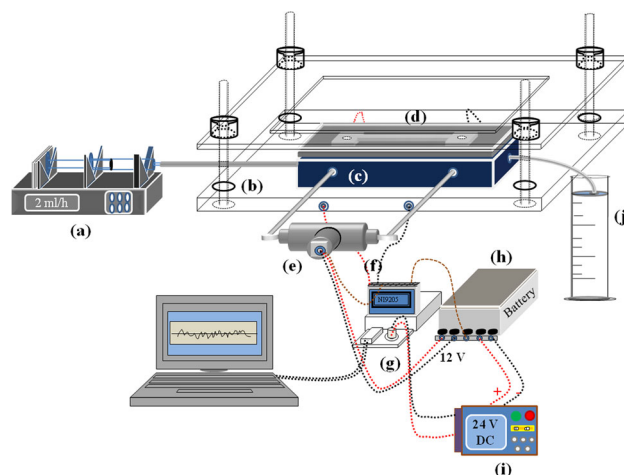


Fig. 1 Schematic diagram of the microfluidic experimental setup; (a) syringe pump, (b) metallic assembly, (c) Teflon sample holder, (d) Si microchannel, (e) differential pressure transducer, (f) K-type thermocouples, (g) DAQ system, (h) 12-V acid battery, (i) 24 V DC power supply and, (j) measuring jar. Dimensions shown are not to scale

holder by matching the inlet and outlet ports of the sample to that of the holder. The whole assembly was tightened with metal screws with “O” rings sandwiched between the sample and the holder.

2.3 Stack preparation in microchannels

The Si microchannel surface was functionalized by a stack of molecular layers as reported earlier (Rathor and Panda 2009; Kumar et al. 2011; Chepyala and Panda 2013), and except for the hydrolysis step, all other steps were carried in situ in the microfluidic setup. Briefly, the microchannel samples were hydrolyzed in 3:1 vol% Piranha solution at 130 ± 5 °C for 1 h by placing the samples at an angle of 45° to allow the capillary flow of the Piranha solution inside the microchannel. This approach was followed to avoid the hydrolysis of the entire sample by complete immersion in the solution. Later, these samples were thoroughly rinsed and dried by flowing the DI water and nitrogen through the microchannels and kept in a vacuum oven at 105 °C for 1 h. After that, the microchannels were silanized by flowing 3 % of either APTES or TMSPDEA or TMSPDETA in toluene as solvent for 2 h and then rinsed thrice with toluene and once with ethanol by flowing each one of the liquid for 10 min followed by drying with the N₂ gas for 10 min. The microchannels were then cross-linked by flowing 2.5 vol% glutaraldehyde in ethanol as a solvent for 1 h, followed by rinsing once with ethanol and DI water and thrice with PBS for 10 min each. The samples were then dried by flowing N₂ gas for 10 min. Finally, the microchannels were immobilized with the antibody of interest (i.e., anti-BSA or anti-PSA or anti-CRP) by flowing PBS solution containing 1 µg/ml of antibodies for 1 h at room temperature. The samples were rinsed for 10 min by flowing PBS solution followed by drying with N₂ gas. In each stage, a fresh set of tubings was used to ensure no contamination from the earlier process steps.

2.4 Characterization

2.4.1 Profilometer

Characterization of the microchannels was done prior to anodic bonding by an XP-Plus Surface Profilometer (Ambios Technology Inc, USA). The scanning was carried out at three or more different locations across and along the channel to measure the geometrical features and surface roughness. The average RMS roughness was measured as 34.3 nm and, 35.1 nm for the 100 µm and the 65 µm microchannels, respectively.

2.4.2 SEM

Scanning electron microscope (FEI, USA) was used to obtain the cross-sectional image of the Si microchannel.

2.4.3 Fluorescence microscopy

Presence of the immobilized antibodies in the Si microchannels was confirmed by imaging the FITC-tagged antibodies by fluorescence microscopy (Leica Microsystems Fluorescence Microscope, Germany).

2.5 Validation of experimental setup

Validation of the experimental setup has been done in two stages; in the first stage (Sect. 2.5.1), the electrical instrumentation was validated and in the second (Sect. 2.5.2), the fluid flow was validated by carrying out conventional pressure drop experiments with known dimensions of a stainless steel tube.

2.5.1 Electrical instrumentation

The voltage fluctuation of the DC power supply was measured by using an oscilloscope, before and after connecting the pressure transducers and DAQ chords, and the measured ripple factor was negligibly small (<2 mV). A rechargeable acid battery of 12 V was used to supply ripple free DC power to the differential pressure transducers.

2.5.2 Validation by fluid flow in a steel tube

A circular stainless steel tube of length 0.704 m was chosen to validate the experimental setup. Several measurements were made across the steel tube and the resulting averaged internal diameter of the tube was 0.00096 m (L/D ratio 733.3) as seen from SEM image (not shown here). The steel tube was thoroughly cleaned by flowing IPA and DI water at high pressures for 15 min each and later dried by flowing N₂ gas for 10 min. The steel tube was connected between two Perspex sheets at the upstream and the downstream side having two large reservoirs (diameter: 15 mm, depth: 6.5 mm) with fluid access ports (outer diameter: 0.5 mm) to the pressure transducer and the syringe pump. The pressure drop experiments were carried out by flowing DI water at constant flow rates from 10 to 100 ml/h and recording the resulting pressure drop using a LABVIEW program. The flow rates were measured by collecting the exit liquid in a measuring jar for a given time, with the liquid mass weighed in a high precision microbalance and then converted to volumetric flow rate by using the density of the liquid at an average temperature of

the flowing liquid. The Reynolds number ranged from 2 to 40, and the experimental friction constant (fRe) was calculated and compared with the theoretical value.

2.6 Pressure drop experiments in Si microchannels

The pressure drop experiments in the Si microchannels were carried by aligning the microchannel on the Teflon channel holder assembly with its inlet and outlet ports and then tightening the test assembly with metal screws to the permissible pressure limits. The test assembly was connected with 0.5 mm Teflon tubings to the high-pressure syringe pump (PHD 2000 ULTRA) to pump the liquids of interest. The pressure drop was measured between the upstream and downstream ports by using a calibrated high precision differential pressure transducer (OMEGA) of the appropriate range: 0–0.36 psi (model: PX409-10WDWU5V), 0–0.25 psi (model: PX409-2.5DWU5V) with accuracy of 0.08 % linearity and 0–5 psi (model: PX26-005DV) with accuracy of ± 0.25 %. The pressure transducer was set to zero each time prior to the actual measurement of the pressure drop and the measured values were collected by the DAQ system (NI-9205), recorded by the LABVIEW program.

The pressure drop measurements in the stack of functionalized microchannels were carried out by flowing liquids of different polarities, i.e., DI water (1.85 D), methanol (1.69 D), and IPA (1.66 D) at different flow rates (1–50 ml/h) to obtain the Re in the range of 1–55. Use of other liquids was limited by handling issues. The exit tube of the test assembly was kept in contact with a constant liquid column in a 5-ml graduated cylinder to eliminate the effects of surface tension at the exit (Judy et al. 2002). In situ measurement of the flowing liquid's temperature accurate to 0.5 °C, at the upstream and downstream plenums, was carried out by using K-type thermocouples (model: 5SRTC-TT-K-36-72, OMEGA) connected to the DAQ system (NI-9211) with the LABVIEW program. The average of the inlet and the outlet temperatures was used to determine the physical properties of the liquids. The Si microchannels used in this study have hydraulic diameters of 98.56 and 66.84 μm , and for the engineering approximation, they are referred to subsequently as the 100- μm and the 65- μm microchannels, respectively. The microchannels had a length of 10 mm, plenum sizes of 5 mm \times 5 mm, plenum depths of 66.54, and 58.82 μm , respectively, for the 100 and 65 μm microchannels. An exemplary cross-sectional image of an anisotropically etched microchannel of about 100 μm hydraulic diameter is shown in Fig. 2. A separate set of tubings were used for microchannel functionalization and for the fluid flow experiments, and care was taken to avoid any possible cross-contamination by flushing the test assembly with

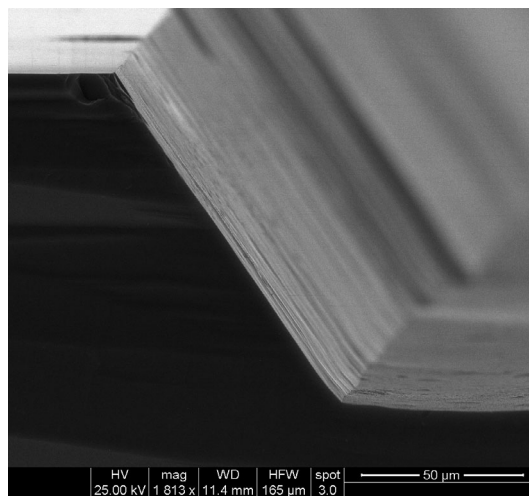


Fig. 2 Exemplary cross-sectional SEM image of an anisotropically etched Si microchannel of about 100 μm hydraulic diameter

suitable liquids for prolonged time and proper drying with N_2 gas. Importantly, the same microchannel of a single hydraulic diameter was regenerated and reused for each stage of functionalization and fluid flow experiments in a single test assembly. This was done to avoid any possible errors in the measurement of pressure drop due to use of different fabricated microchannels even for the same design. The measurements were taken in triplicate and the error signifies one standard deviation.

3 Results and discussion

3.1 Validation results

We used the classical Hagen-Poiseuille theory to validate the experimental setup by conducting pressure drop experiments in a stainless steel tube with known dimensions. The measured pressure drop of flowing water in the steel tube was found to vary linearly with the flow rate, and the entrance effects were ignored due to the large L/D ratio (of 733.3). The pressure drop data along with other parameters were used to calculate the experimental friction constant (fRe) as per the equation,

$$fRe = \frac{2\Delta P D_h^2}{L\mu V} \quad (1)$$

and compared with the theoretically calculated friction constant. Here, f is the coefficient of flow resistance known as the friction factor, ΔP is the measured pressure drop, D_h is the hydraulic diameter, L is the length of the tube, μ is the dynamic viscosity of the fluid, and V is the average velocity. The mean value of fRe was 66.50 ± 0.5 , close (within 3.7 %) to the theoretical value of 64. This validated our measurement setup.

Table 1 Average fRe values of the non-functionalized and various functionalized stages in the stack in the 100- μm microchannel

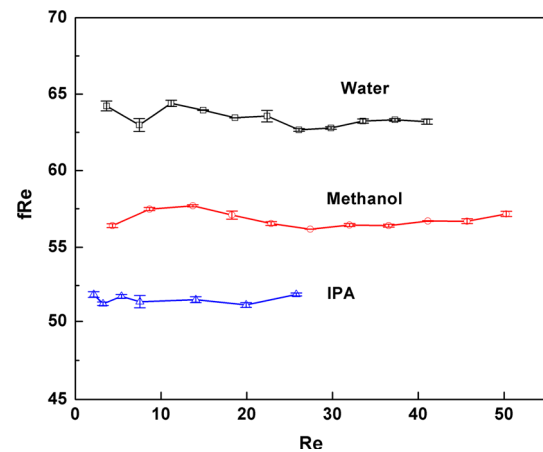
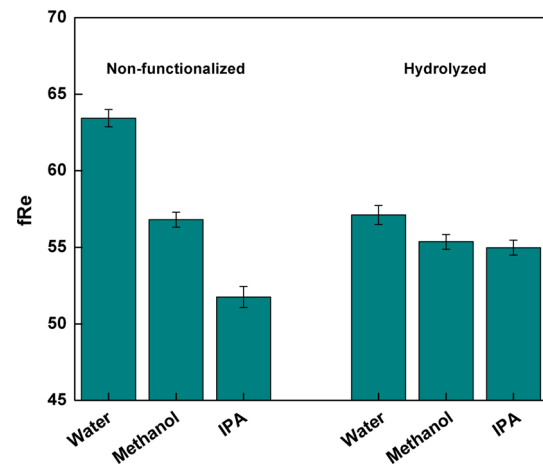
Stack	fRe		
	Water	Methanol	IPA
Non-functionalized	63.43 ± 0.56	56.79 ± 0.49	51.76 ± 0.69
Hydrolyzed	57.10 ± 0.62	55.36 ± 0.47	54.98 ± 0.48
Silanized			
APTES	58.66 ± 0.60	56.65 ± 0.41	53.80 ± 0.48
TMSPEDA	71.32 ± 2.68	57.80 ± 1.29	59.14 ± 0.42
TMSPDETA	59.41 ± 1.02	54.97 ± 0.76	58.68 ± 0.97
Antibody immobilization			
Anti-BSA			
APTES	59.50 ± 0.30	55.20 ± 0.46	52.20 ± 0.59
TMSPEDA	61.34 ± 0.48	59.80 ± 0.50	60.45 ± 0.64
TMSPDETA	58.38 ± 0.80	55.31 ± 0.52	56.29 ± 0.28
Anti-PSA			
APTES	58.53 ± 0.60	56.75 ± 0.45	56.20 ± 0.30
TMSPEDA	59.80 ± 0.50	55.21 ± 0.25	56.32 ± 0.24
TMSPDETA	58.68 ± 0.70	56.27 ± 0.88	57.25 ± 0.27
Anti-CRP			
APTES	58.88 ± 0.57	56.09 ± 0.33	54.02 ± 0.47
TMSPEDA	60.72 ± 0.70	57.67 ± 0.23	57.29 ± 0.36
TMSPDETA	59.11 ± 0.51	57.69 ± 0.60	56.52 ± 0.48

3.2 Fluid flow results in Si microchannels

The fluid flow experiments were carried out in the 100- μm Si microchannel and to verify the obtained results, similar experiments for some of the conditions were also performed in the 65- μm microchannel. The measured pressure drop along with flow rate data and hydraulic diameters of the non-circular microchannels used in this study were substituted in Eq. (1) to calculate the fRe values, as has been used in many reports (Xiong 2011; Weilin et al. 2000) for laminar flows. The analysis of the fRe values calculated by flowing liquids of different polarities through the non-functionalized (Sect. 3.2.1) and the functionalized microchannels (Sect. 3.2.2) with different molecular layers including the antibodies are presented here. The average fRe values for the different liquids flowing in the non-functionalized and functionalized 100- μm microchannel are summarized in Table 1.

3.2.1 fRe values in non-functionalized microchannels

The plot of fRe versus Re for the non-functionalized 100- μm microchannel for the flow of different liquids is shown in Fig. 3. The fRe values are considered to be nearly constant over the entire range (1–50) of Re studied for all these liquids.

**Fig. 3** Measured fRe versus Re obtained in the non-functionalized 100- μm microchannel for the flow of different liquids**Fig. 4** Measured fRe values of the 100- μm hydrolyzed microchannel along with the fRe values of non-functionalized microchannel. Liquid polarities are in the order of water > methanol > IPA

The average fRe values for DI water, methanol, and IPA are 63.43 ± 0.56 , 56.79 ± 0.49 , and 51.76 ± 0.69 , respectively (Table 1; Fig. 4). The order of the fRe values obtained here, i.e., water > methanol > IPA, was also seen in the 65- μm microchannel (water: 61.52 ± 0.61 > methanol: 53.86 ± 0.56 > IPA: 50.30 ± 0.47). We attribute this trend to the stronger interaction between the liquids of higher polarity with the solid surface (Fu-Bing and Zhong 2009), and these results are in accordance with the results of Kulinsky et al. (1999), who experimentally found electrokinetic retardation of polar fluids (water, ethyl alcohol, *n*-propyl alcohol) in 90–100- μm microchannels, suggesting that liquids with higher polarities experience a greater frictional resistance. Also, an experimental verification of a model based on micropolar behavior proposed by Papautsky et al. (1999b) using Si microchannels (600 μm width, 30 μm height) at Reynolds numbers in the range 1–20 showed increased frictional resistance to the liquids with

higher polarities. Our work contradicts the work of others (Judy et al. 2002; Phares and Smedley 2004; Sharp and Adrian 2004) who did not find any effect of the polarities of the liquids on the frictional resistance. The effect of surface free energies on the friction constants will be studied in the subsequent sections.

Here, based on the aspect ratio and the angle of the trapezoidal microchannels, the theoretical value of fRe is 96 (Shah and London 1978; Morini 2004) for both the microchannels, and the fRe values obtained for both the 100- μm and the 65- μm microchannels for the flow of different liquids were smaller than the theoretically predicted fRe value. There are contradictory reports in the literature regarding the experimental fRe values in comparison to the theoretically predicted values, with some studies showing higher (Weilin et al. 2000; Wu and Cheng 2003a) and some showing lower (Pit et al. 2000; Bonaccorso et al. 2002) values. We have not looked on this aspect here, but rather have focused on understanding the solid–liquid interactions by relative comparison of the fRe values in each functionalized stage.

3.2.2 fRe values in functionalized microchannels

3.2.2.1 Hydrolyzed microchannel The fRe values obtained in the hydrolyzed 100- μm microchannel were almost constant over the range of Re (1.7–57) studied for all the liquids (fRe versus Re plot not shown here), and the average fRe values are shown in Table 1. From Table 1, it is seen that the average fRe values for DI water, methanol, and IPA are 57.10 ± 0.62 , 55.36 ± 0.47 , and 54.98 ± 0.48 , respectively, and these values are plotted in Fig. 4 along with the values obtained in the non-functionalized microchannel. The results show that the fRe values obtained for 100- μm hydrolyzed microchannel while flowing different liquids is in the order of the liquid polarities (i.e., water > methanol > IPA, though the values for methanol and IPA were within experimental error) and this behavior is similar to that seen in the non-functionalized microchannel. Similarly, in the 65- μm hydrolyzed microchannel, the average fRe values for DI water, methanol, and IPA are 55.19 ± 0.5 , 52.50 ± 0.8 , and 51.25 ± 0.7 , respectively, and the fRe values is in the order of the liquid polarities (again with the fRe values of methanol and IPA being within experimental error). Thus, liquids with higher polarities yield stronger solid–liquid interactions resulting in increased frictional resistance to the liquid flow. For all the three liquids flowing in the 100- μm and the 65- μm hydrolyzed microchannels, the average fRe values were lower than those in the corresponding non-functionalized microchannels (Fig. 4), except for IPA both in the 100- μm and the 65- μm microchannels, possible reason of which is discussed subsequently.

We compared the fRe values of the functionalized microchannels obtained by flowing liquids of different properties, with the surface free energies of the Si surfaces of these stages as studied in our previous work (Chepyala and Panda 2013), to see if there are any correlations between the fRe values and surface free energies. The trapezoidal microchannels used in this study comprise three surfaces of etched Si, having an RMS surface roughness of the order ~ 34 nm and the other surface being a smooth Pyrex glass. And hence, the microchannel is a combination of smooth and relatively rough surfaces; therefore, instead of correlating the fRe values with either of only non- or nanotextured Si surface free energies, we used the range/average of surface free energies.

In Fig. 5, the fRe values of the hydrolyzed surface and the non-functionalized surface are plotted for each liquid along with the surface free energies. It is seen that the higher surface free energies of the hydrolyzed Si surfaces (63 – 65 mJ/m^2) compared to that of the non-functionalized surfaces (48 – 50 mJ/m^2) (Chepyala and Panda 2013) are intuitively expected to result in a higher fRe values due to the stronger solid–liquid interactions (Fu-Bing and Zhong 2009). However, the observed behavior was counter intuitive for DI water and methanol. A possible reason could be a fluid layering at the surface, where the higher surface free energy could have resulted in the formation of one or more layers (Sun et al. 2002; Cottin-Bizonne et al. 2005; Schmatko et al. 2005) of immobile-oriented polar liquid molecules (Urbanek et al. 1993; Sun et al. 2002) over which the bulk of the fluid molecules experience a “slip” resulting in a reduced drag (i.e., decreased fluid friction). This phenomenon is supported by the results of Bonaccorso et al. (2002), who reported slip lengths of 8–9 nm on completely wetting mica surfaces (surface free energy not

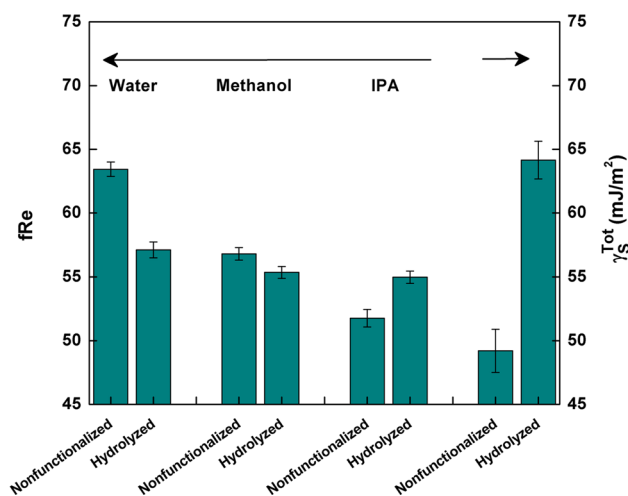


Fig. 5 Measured fRe values of the hydrolyzed and the non-functionalized 100- μm microchannel for each liquid along with the surface free energies

reported) in aqueous electrolyte solutions by using a colloidal probe technique and stated that the electrokinetic repulsion between the completely wetting surfaces and the liquid molecules resulted in decreased solid–liquid interactions. Similarly, we believe that the higher surface free energy in the hydrolyzed microchannel has provided sufficient strength of attraction to the small-chain liquid molecules (water and methanol) which formed layers on the surface. Even non-polar liquids of longer chain lengths such as squalane and hexadecane have shown to form fluid layering on bare sapphire α -Al₂O₃ hydrophilic surface with higher surface free energy ($\gamma_s^{\text{Tot}} > 72 \text{ mJ/m}^2$) (Schmatko et al. 2005). Similarly, Sun et al. (2002) also showed a layered structure of 1-propanol of at least 3 molecular layers in confined geometries of mica (surface free energy not reported) by using a colloidal probe technique and found significant slip of 10–14 nm. An interesting point to observe from the results of Schmatko et al. (2005) is that the higher surface free energies of mica ($\gamma_s^{\text{Tot}} > 72 \text{ mJ/m}^2$) have the ability to pull even the long-chain non-polar liquids toward the surface, and similar phenomena might have occurred in case of fluid layering of 1-propanol in the experiments of Sun et al. (2002) where the surface free energies may have been comparable. In our experiments, since the surface free energy of hydrolyzed surface is of the order of 63–65 mJ/m², this might not have been sufficient to affect the relatively bulky IPA molecules to form layering as seen in the other polar liquids of smaller molecular size. Therefore, this study shows that while smaller liquid molecules (water, methanol) are affected by the high solid surface free energy causing layering, bulky/larger fluid molecules (IPA) are not. There are several simulations and experimental studies available which focus on the fluid–solid interactions and calculate the resulting slip lengths to understand the strength of the interactions (Ulmanella and Ho 2008; Choi et al. 2006). Calculation of slip lengths for these functionalized stages is beyond the scope of the present work.

3.2.2.2 Silanized microchannel The average fRe values obtained in the 100- μm microchannel functionalized with aminosilanes of different chain lengths (APTES: $\sim 5 \text{ \AA}$, TMSPEDA: $\sim 8 \text{ \AA}$ and TMSPDETA: $\sim 10 \text{ \AA}$) are shown in Table 1, and the values were nearly constant over the entire range of Re (1–53) studied for all the liquids (fRe versus Re plot not shown here). In Fig. 6, measured fRe values of the 100- μm microchannel functionalized with different silanes are shown for different polar liquids. From Table 1 and Fig. 6, it is seen that the average fRe values for DI water, methanol, and IPA flowing in the microchannel functionalized with APTES were 58.66 ± 0.6 , 56.65 ± 0.41 , and 53.8 ± 0.48 , respectively. The behavior of the fRe values obtained in the microchannels functionalized

with short-chain APTES molecules are in the order of the liquid polarities (water > methanol > IPA) indicating that liquids with higher polarities result in stronger solid–liquid interactions. Similarly, the effect of liquid polarity can be seen in TMSPEDA- and TMSPDETA-functionalized microchannels, though not as distinctly as seen with APTES, where the average fRe values of water were higher than either methanol or IPA (but within experimental error for TMSPDETA). However, the average fRe values of IPA in TMSPEDA- and TMSPDETA-functionalized microchannels were higher than methanol (within experimental error for TMSPEDA), and a possible reason could be the different interactions between the bulkier liquid molecules and surface bound longer-chain molecules of different orientation. These results are supported by Schmatko et al. (2005) who reported that the solid–liquid interactions and the local velocity at the solid wall would be affected by small changes in the shape of the molecules of the fluid. These results indicate that on silanized surfaces, the relationship between the fRe values and the liquid polarities is clearer for relatively smaller liquid/solid molecules but not for the bulkier ones.

In Fig. 7, the fRe values of the 100- μm microchannel functionalized with different silanes (APTES, TMSPEDA, and TMSPDETA) were recast and compared with the surfaces free energies to see any possible correlation between them. Since, the surface free energies of different silane-functionalized surfaces (47–52 mJ/m²) were smaller (Chepyala and Panda 2013) than the hydrolyzed surface (63–65 mJ/m²), any behavior attributed to fluid layering is not expected. From Fig. 7, it is seen that the TMSPEDA gives highest average fRe values for all three liquids (with fRe values of IPA on TMSPEDA and TMSPDETA being within experimental error). As the surface free energy of

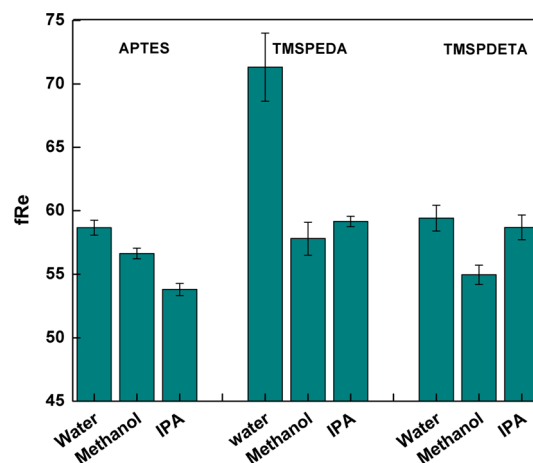


Fig. 6 Measured fRe values of APTES-, TMSPEDA-, and TMSPDETA-functionalized layers in the 100- μm microchannel. Liquid polarities are in the order of water > methanol > IPA

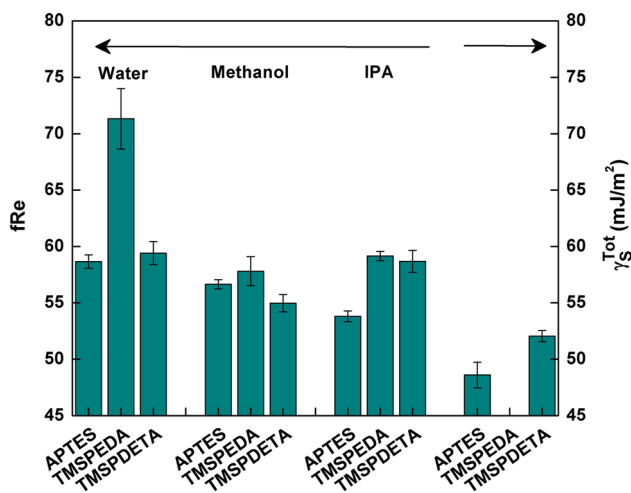


Fig. 7 Measured fRe values of APTES, TMSPEDA, and TMSPD-ETA in the 100-µm microchannel for each liquid along with the surface free energies

the TMSPEDA-functionalized surface could not be calculated (Chepyala and Panda 2013), we compare the surface free energies of the APTES- and TMSPDETA-functionalized surfaces. Since the surface free energy of the TMSPDETA (51.7–52.4 mJ/m²) was higher than the APTES (47.8–49.4 mJ/m²), higher values of fRe were seen on the TMSPDETA-functionalized microchannel surface for water and IPA (but not for methanol, the reason of which is not clear). Another observation from Fig. 7 is that in all the functionalized stages and for all the liquids, the average fRe values of APTES were consistently smaller than the TMSPEDA (within error limits for methanol on APTES and TMSPEDA). Based on the chain lengths of the three silanes, it is expected that TMSPDETA should have yielded higher fRe values than TMSPEDA, which, however, is not seen. The possible reason could be that the longer chain length molecule TMSPDETA could have bent toward the surface (Park and Kim 1994) resulting in different orientations, and the different extent of the bending (Yakovleva et al. 2002) could have confounded the results.

3.2.2.3 Antibody-immobilized microchannel The average fRe values obtained in the 100-µm microchannel immobilized with three different antibodies (anti-BSA, anti-PSA, and anti-CRP) on three different silanes are shown in Table 1. Before performing the fluid flow experiments in the antibody-immobilized microchannel, presence of antibodies inside the microchannel was confirmed by imaging FITC-tagged antibodies (used for the verification purpose only) by using fluorescence microscopy, and a sample image of the anti-PSA tagged with FITC in the 100-µm microchannel is shown in Fig. 8.

The average fRe values obtained in the 100-µm microchannel immobilized with anti-BSA on different silanes

(APTES, TMSPEDA, and TMSPDETA) are shown in Table 1 and the values were reasonably constant over the range of the Re (1–50) studied for all the liquids. A sample plot of the fRe values for anti-BSA- on APTES-functionalized microchannel is shown in Fig. 9.

The fRe values for the flow of water (59.50 ± 0.30), methanol (55.20 ± 0.46), and IPA (52.20 ± 0.59) through the anti-BSA immobilized on to APTES microchannel are in the order of their liquid polarities (water > methanol > IPA) as seen in Fig. 10, indicating that the higher fRe values were obtained with the liquids of higher polarities. Similar behavior was also seen with the other antibodies immobilized on to APTES (Figs. 11, 12), with the fRe values of water: 58.53 ± 0.60, methanol: 56.75 ± 0.45, and IPA: 56.20 ± 0.30 (values for methanol and IPA being within experimental error) on anti-PSA and

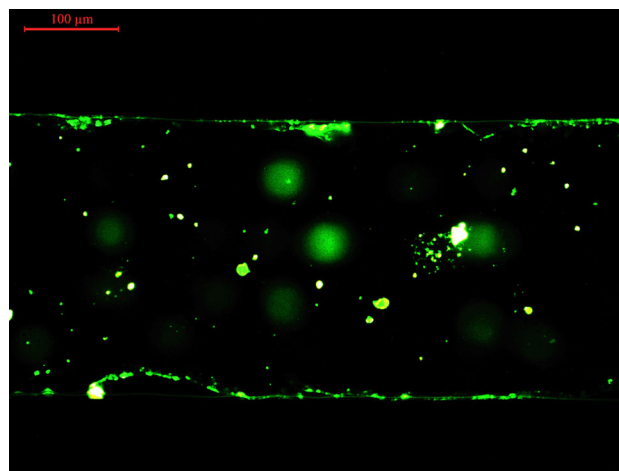


Fig. 8 Fluorescence image of the anti-PSA antibody tagged with FITC immobilized in the 100-µm microchannel. The image was taken through the 1.5-mm-thick Pyrex glass bonded to the microchannel

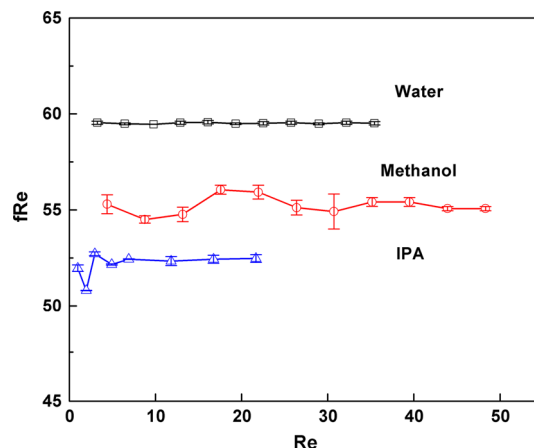


Fig. 9 Measured fRe versus Re values of different liquids flowing through the 100-µm microchannel immobilized with anti-BSA antibodies on to APTES

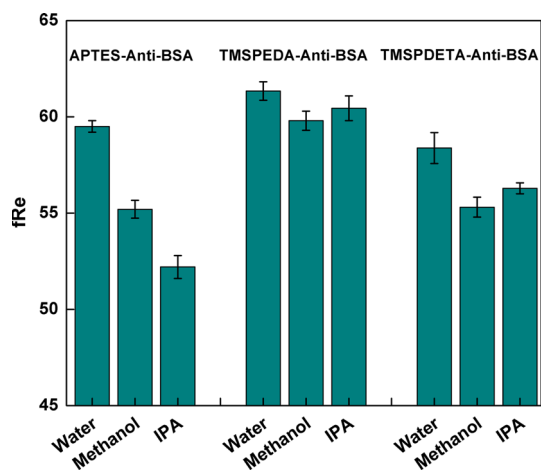


Fig. 10 Measured fRe values of different liquids flowing through the 100- μm microchannel immobilized with anti-BSA on to APTES, TMSPEDA, and TMSPDETA

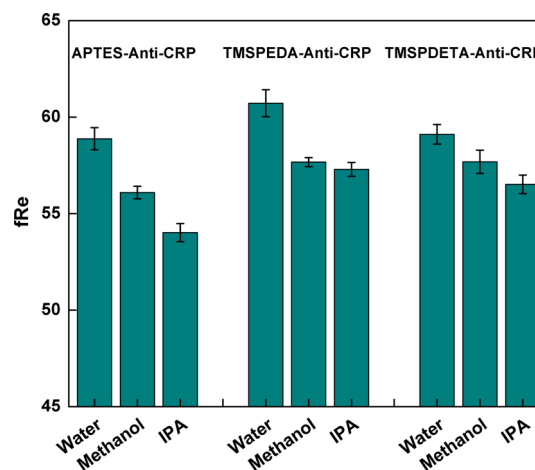


Fig. 12 Measured fRe values of different liquids flowing through the 100- μm microchannel immobilized with anti-CRP on to APTES, TMSPEDA, and TMSPDETA

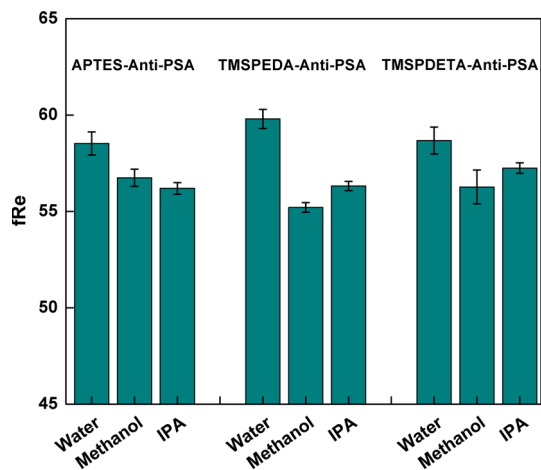


Fig. 11 Measured fRe values of different liquids flowing through the 100- μm microchannel immobilized with anti-PSA on to APTES, TMSPEDA, and TMSPDETA

values of water: 58.88 ± 0.57 , methanol: 56.09 ± 0.33 , and IPA: 54.02 ± 0.47 on anti-CRP. Thus, in microchannels immobilized with different antibodies on to short chain (APTES) molecules, liquids with higher polarities result in stronger solid–liquid interactions.

From Figs. 10, 11, and 12, it is seen that the average fRe values for flow of water in anti-BSA, anti-PSA, and anti-CRP antibodies immobilized on to TMSPEDA and TMSPDETA were higher than that of methanol and IPA. The relation between the fRe values for methanol and IPA was not clear, with higher average values with IPA seen with anti-BSA and anti-PSA, as seen with silanes, but not with anti-CRP. These results suggest that for the flow of bulkier liquids (IPA) over different antibodies immobilized with longer chain molecules, the flow properties were affected not only by the liquid polarities but also were confounded by other factors.

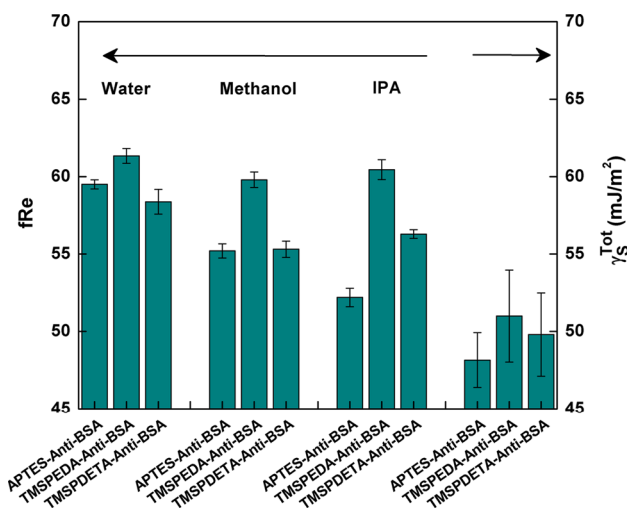


Fig. 13 Measured fRe values of anti-BSA on APTES, TMSPEDA, and TMSPDETA shown for each of the liquid flowing through the 100- μm microchannel along with the surface free energies

Now the data from Figs. 10, 11 and 12 were recast and presented along with the surface free energies (Chepyala and Panda 2013) in Figs. 13, 14 and 15, respectively. From Fig. 13, it is seen that for all three liquids, the average surface free energy of anti-BSA immobilized on TMSPEDA (61.3 ± 0.48 for water, 59.50 ± 0.50 for methanol, and 60.45 ± 0.64 for IPA) was higher than that on APTES or TMSPDETA. This behavior is similar to that seen for silanes (Fig. 7). However, the relationship between the fRe values with APTES and TMSPDETA is not clear with the values for TMSPDETA being lower with water, comparable with methanol and higher with IPA. As discussed earlier, the bending of the longer chain silane to different extents could have confounded the results.

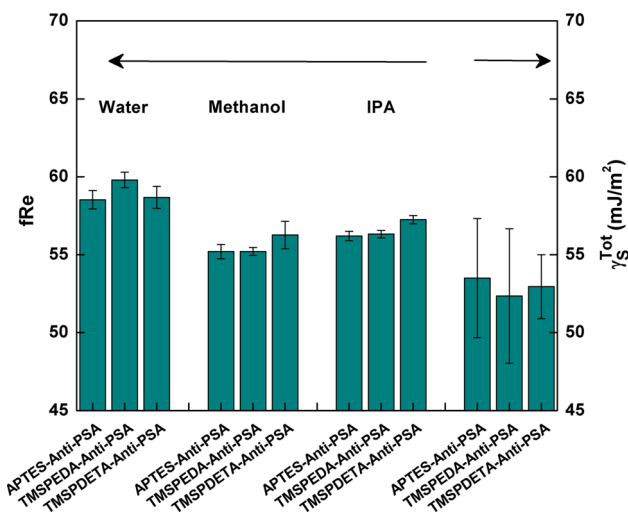


Fig. 14 Measured *fRe* values of anti-PSA on APTES, TMSPEDA, and TMSPDETA shown for each of the liquid flowing through the 100- μm microchannel along with the surface free energies

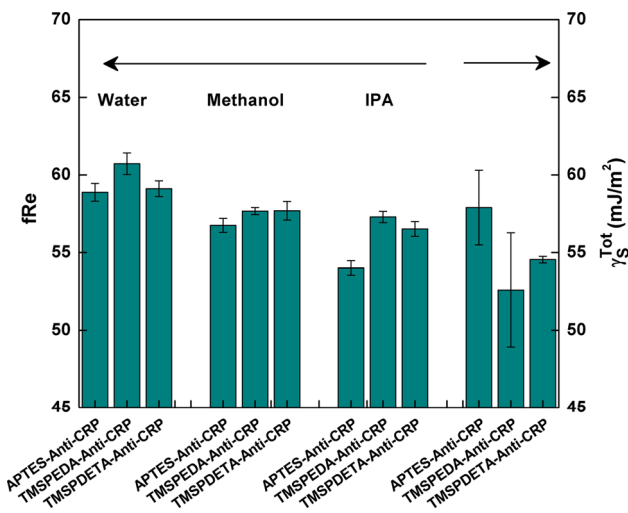


Fig. 15 Measured *fRe* values of anti-CRP on APTES, TMSPEDA, and TMSPDETA shown for each of the liquid flowing through the 100- μm microchannel along with the surface free energies

While some correlation between the surface free energies and the *fRe* values were seen for anti-BSA, no clear trends were seen for anti-PSA and anti-CRP. There could be several reasons for this. In our earlier work (Chepyala and Panda 2013), we had observed that the surface free energies (averaged over non- and nanotextured surfaces) were in the order anti-BSA < anti-PSA < anti-CRP immobilized on APTES and on TMSPEDA. At this point of time, we speculate that the higher surface free energies of anti-PSA and anti-CRP could have resulted in a loss of the correlation. Also, the orientation of the antibodies could be a factor with a possibility of the intermediate molecular weight anti-BSA (67 kDa) having a more controlled orientation than

that of anti-PSA (33 kDa) or anti-CRP (120 kDa). The effect of antibody orientation based on molecular weights on fluid flow can be better understood by utilizing site-directed proteins for immobilization and is a subject of future work. Nevertheless, the identification of the range of *fRe* values for anti-PSA and anti-CRP could be helpful in designing appropriate microfluidic immunosensors.

Since the diffusion of the antigens in the carrier fluid to the antibody-immobilized surfaces is governed by the velocity profile (Cottin-Bizonne et al. 2004, Zimmermann et al. 2005), the polarity of the liquid would affect the velocity profile which again would affect the antigen–antibody interactions. Therefore, we believe that the knowledge generated here could help in better understanding of the fluid flow phenomena thereby guiding measures for more effective fluid flow, leading to improved designs of microfluidic immunosensors.

4 Conclusions

We have carried out a systematic study to characterize the fluid flow of the different polar liquids in the trapezoidal Si microchannels of about 100 and 65 μm hydraulic diameters, functionalized with different chain lengths of amino-silanes along with three different antibodies immobilized through these molecular layers. Friction constants were calculated for each stage of functionalization (which includes the antibody surfaces) from pressure drop measurements of these liquids flowing through the microchannels over a range (1–50) of Reynolds numbers. The friction constants were analyzed to see any correlation with the liquid polarities and the solid surface free energies to understand the liquid–solid interactions. Overall, increased friction constants with liquids of higher polarities were seen for almost all the functionalized surfaces and these were attributed to the stronger solid–liquid interactions. However, on the high surface energy-hydrolyzed surfaces, an opposite behavior was seen for relatively smaller liquid molecules (water and methanol), and this was attributed to the possible fluid layering. In microchannels functionalized with the longer chain silane, results were confounded due to possible bending to different extents of the silane. Similar confounding results were seen with bulkier liquid molecules. A reasonable correlation of the surface free energies with the friction constants was seen for most surfaces, including the anti-BSA immobilized on to different silanes. However, no clear trends were seen for the anti-PSA and the anti-CRP surfaces, and we speculate that higher surface free energies of anti-PSA and anti-CRP could have contributed to the loss of correlation along with the orientation effects. Overall, values of the measured friction constants and the knowledge of the solid–liquid

obtained interactions could assist improved designs of microfluidic immunosensors.

Acknowledgments The authors gratefully acknowledge the financial support of the Department of Science and Technology, India. The help of Dr. Satyendra Kumar with some experiments is acknowledged.

References

- Andrade JD, Hlady V, Wei AP (1992) Adsorption of complex proteins at interfaces. *Pure Appl Chem* 64(11):1777–1781
- Aubin J, Ferrando M, Jiricny V (2010) Current methods for characterising mixing and flow in microchannels. *Chem Eng Sci* 65(6):2065–2093
- Bahrami M, Yovanovich MM, Culham JR (2006) Pressure drop of fully developed, laminar flow in rough microtubes. *J Fluids Eng* 128(3):632–637
- Bahrami M, Yovanovich MM, Culham JR (2007) A novel solution for pressure drop in singly connected microchannels of arbitrary cross-section. *Int J Heat Mass Transf* 50(13–14):2492–2502
- Bernard A, Renault JP, Michel B, Bosshard HR, Delamarche E (2000) Microcontact printing of proteins. *Adv Mater* 12:1067–1070
- Bonaccorso E, Kappl M, Butt HJ (2002) Hydrodynamic force measurements: boundary slip of water on hydrophilic surfaces and electrokinetic effects. *Phys Rev Lett* 88(7):076103
- Brash JL (1987) Protein adsorption at the solid-solution interface in relation to blood-material interactions, vol 343. *Proteins at interfaces physicochemical and biochemical studies*. American Chemical Society, Washington, DC
- Brutin D, Tadrast L (2003) Experimental friction factor of a liquid flow in microtubes. *Phys Fluids* 15(3):653–661
- Brutin D, Topin F, Tadrast L (2003) Transient method for the liquid laminar flow friction factor in microtubes. *AIChE J* 49(11):2759–2767
- Cappelletti G, Arduzzone S, Meroni D, Soliveri G, Ceotto M, Biaggi C, Benaglia M, Raimondi L (2013) Wettability of bare and fluorinated silanes: a combined approach based on surface free energy evaluations and dipole moment calculations. *J Colloid Interface Sci* 389(1):284–291
- Capretto L, Cheng W, Hill M, Zhang X (2011) Micromixing within microfluidic devices. *Top Curr Chem* 304:27–68
- Celata GP, Cumo M, McPhail S, Zummo G (2006) Characterization of fluid dynamic behaviour and channel wall effects in microtube. *Int J Heat Fluid Flow* 27(1):135–143
- Chang H-I, Wang Y (2011) Cell responses to surface and architecture of tissue engineering scaffolds. In: Eberli D (ed) *Regenerative medicine and tissue engineering-cells and biomaterials*, ISBN: 978-953-307-663-8, InTech. doi:10.5772/21983
- Chao QU, Fu-Quan S (2011) Flow characteristics of deionized water in microtubes absorbing fluoro-alkyl silanes. *Chin Phys Lett* 28(10):104701
- Chen X, Cui D, Liu C, Li H, Chen J (2007) Continuous flow microfluidic device for cell separation, cell lysis and DNA purification. *Anal Chim Acta* 584(2):237–243
- Chepyala R, Panda S (2013) Tunable surface free energies of functionalized molecular layers on Si surfaces for microfluidic immunosensor applications. *Appl Surf Sci* 271:77–85
- Choi CH, Westin KJA, Breuer KS (2003) Apparent slip flows in hydrophilic and hydrophobic microchannels. *Phys Fluids* 15(10):2897–2902
- Choi CH, Ulmanella U, Kim J, Ho CM, Kim CJ (2006) Effective slip and friction reduction in nanograted superhydrophobic microchannels. *Phys Fluids* 18(8):087105
- Cottin-Bizonne C, Barentin C, Charlaix E, Bocquet L, Barrat J-L (2004) Dynamics of simple liquids at heterogeneous surfaces: molecular-dynamics simulations and hydrodynamic description. *Eur Phys J E* 15:427–438
- Cottin-Bizonne C, Cross B, Steinberger A, Charlaix E (2005) Boundary slip on smooth hydrophobic surfaces: intrinsic effects and possible artifacts. *Phys Rev Lett* 94(5):056102
- Falconnet D, Csucs G, Grandin HM, Tex M (2006) Surface engineering approaches to micropattern surfaces for cell-based assays. *Biomaterials* 27(16):3044–3063
- Fu-Bing B, Zhong LJ (2009) Effect of molecular interactions between the solid wall and liquid on the flow properties in microtubes. *Chin Phys Lett* 26(5):056802
- Gamrat G, Marinnet MF, Person SL, Bavière R, Ayela F (2008) An experimental study and modelling of roughness effects on laminar flow in micro-channels. *J Fluid Mech* 594:399–423
- Gan Y, Xu J, Yang Z (2007) An experimental investigation of flow characteristics for laminar flow in silicon microchannels. In: *International conference on power engineering*, Hangzhou, China
- Gao B, Jin G (2005) Study of interaction force between antigen and antibody using flow chamber method. Paper presented at the IEEE engineering in medicine and biology 27th annual conference, Shanghai, China
- García-Hernando N, Acosta-Iborra A, Ruiz-Rivas U, Izquierdo M (2009) Experimental investigation of fluid flow and heat transfer in a single-phase liquid flow micro-heat exchanger. *Int J Heat Mass Transf* 52(23–24):5433–5446
- Greenway GM, Haswell SJ, Morgan DO, Skelton V, Styring P (2000) The use of a novel microreactor for high throughput continuous flow organic synthesis. *Sens Actuators B* 63(3):153–158
- Gubala V, Harris LF, Ricco AJ, Tan MX, Williams DE (2012) Point of care diagnostics: status and future. *Anal Chem* 84(2):487–515
- Hsieh SS, Lin CY (2009) Convective heat transfer in liquid microchannels with hydrophobic and hydrophilic surfaces. *Int J Heat Mass Transf* 52(1–2):260–270
- Hu Y, Werner C, Li D (2003) Influence of three-dimensional roughness on pressure-driven flow through microchannels. *J Fluids Eng* 125(5):871–879
- Hu M, Yan J, He Y, Lu H, Weng L, Song S, Fan C, Wang L (2010) Ultrasensitive, multiplexed detection of cancer biomarkers directly in serum by using a quantum dot-based microfluidic protein chip. *ACS Nano* 4(1):488–494
- Judy J, Maynes D, Webb BW (2002) Characterization of frictional pressure drop for liquid flows through microchannels. *Int J Heat Mass Transf* 45(17):3477–3489
- Jung DR, Kapur R, Adams T, Giuliano KA, Mrksich M, Craighead HG, Taylor DL (2001) Topographical and physicochemical modification of material surface to enable patterning of living cells. *Crit Rev Biotechnol* 21(2):111–154
- Kandlikar SG (2012) History, advances, and challenges in liquid flow and flow boiling heat transfer in microchannels: a critical review. *J Heat Transfer* 134(3):034001
- Kandlikar SG, Schmitt D, Carrano A, Taylor J (2005) Characterization of surface roughness effects on pressure drop in single-phase flow in micro-channels. *Phys Fluids* 17(10):100606
- Keselowsky BG, Collard DM, García AJ (2004) Surface chemistry modulates focal adhesion composition and signaling through changes in integrin binding. *Biomaterials* 25:5947–5954
- Kleinstreuer C, Koo J (2004) Computational analysis of wall roughness effects for liquid flow in micro-conduits. *J Fluids Eng* 126:1–9
- Kockmann N, Kiefer T, Engler M, Woias P (2006) Convective mixing and chemical reactions in microchannels with high flow rates. *Sens Actuators B* 117:495–508

- Koo J, Kleinstreuer C (2004) Viscous dissipation effects in microtubes and microchannels. *Int J Heat Mass Transf* 47(14–16):3159–3169
- Kulinsky L, Wang Y, Ferrari M (1999) Electroviscous effects in microchannels. In: SPIE conference on micro and nanofabricated structures and devices for biomedical environmental applications II San Jose, CA, pp 158–168
- Kumar S, Ch R, Rath D, Panda S (2011) Densities and orientations of antibodies on nano-textured silicon surfaces. *Mater Sci Eng, C* 31(2):370–376
- Lee CY, Chang CL, Wang YN, Fu LM (2011) Microfluidic mixing: a review. *Int J Mol Sci* 12(5):3263–3287
- Li D, Mala GM (1999) Flow characteristics of water in microtubes. *Int J Heat Fluid Flow* 20(2):142–148
- Lina CT, Lin CH (2011) A statistical nanomechanism of biomolecular patterning actuated by surface potential. *J Appl Phys* 109(3):034702
- Malhotra R, Patel V, Chikkaveeriah BV, Munge BS, Cheong SC, Zain RB, Abraham MT, Dey DK, Gutkind JS, Rusling JF (2012) Ultrasensitive detection of cancer biomarkers in the clinic by use of a nanostructured microfluidic array. *Anal Chem* 84(14):6249–6255
- Miller EM, Wheeler AR (2008) A digital microfluidic approach to homogeneous enzyme assays. *Anal Chem* 80(5):1614–1619
- Morini GL (2004) Laminar liquid flow through silicon microchannels. *J Fluids Eng* 126(3):485–489
- Mrksich M, Whitesides GM (1996) Using self-assembled monolayers to understand the interactions of man-made surfaces with proteins and cells. *Annu Rev Biophys Biomol Struct* 25:55–78
- Nayak K, Kulkarni PD, Deepu A, Sitaraman VR, Punidha S, Saha AA, Ravikanth M, Mitra SK, Mukherji S, Rao VR (2007) Patterned microfluidic channels using self-assembled hydroxyphenyl porphyrin monolayer. In: Proceedings of the 7th IEEE international conference on nanotechnology, Hong Kong
- Papautsky I, Gake BK, Mohanty S, Ameel TA, Frazier AB (1999a) Effects of rectangular microchannel aspect ratio on laminar friction constant. In: Proceedings of SPIE-the international society for optical engineering proceedings of the 1999 microfluidic devices and systems II, Santa Clara, CA, pp 147–158
- Papautsky I, Brazzle J, Ameel T, Frazier AB (1999b) Laminar fluid behavior in microchannels using micropolar fluid theory. *Sens Actuators* 73(1–2):101–108
- Park JM, Kim JH (1994) Surface energies of borosilicate glass surfaces modified with n-alkyl silane coupling agents via dynamic contact angle measurements. *J Colloid Interface Sci* 168(1):103–110
- Pfahler J, Harley J, Bau H, Zemel J (1990) Liquid transport in micron and submicron channels. *Sens Actuators* 21(1–3):431–434
- Pfund D, Rector D, Shekariz A, Popescu A, Welty J (2000) Pressure drop measurements in a microchannel. *AIChE J* 46(8):1496–1507
- Phares DJ, Smedley GT (2004) A study of laminar flow of polar liquids through circular microtubes. *Phys Fluids* 16(5):1267–1272
- Pit R, Hervet H, Léger L (2000) Direct experimental evidence of slip in hexadecane: solid interfaces. *Phys Rev Lett* 85(5):980–983
- Rathor N, Panda S (2009) Aminosilane densities on nanotextured silicon. *Mater Sci Eng, C* 29(8):2340–2345
- Salieb-Beugelaar GB, Simone G, Arora A, Philippi A, Manz A (2010) Latest developments in microfluidic cell biology and analysis systems. *Anal Chem* 82(12):4848–4864
- Schmatko T, Hervet H, Leger L (2005) Friction and slip at simple fluid–solid interfaces: the roles of the molecular shape and the solid–liquid interaction. *Phys Rev Lett* 94(24):244501
- Shah RK, London AL (1978) Laminar flow forced convection in ducts. Academic Press, New York
- Sharp KV, Adrian RJ (2004) Transition from laminar to turbulent flow in liquid filled microtubes. *Exp Fluids* 36(5):741–747
- Stroock AD, Dertinger SK, Whitesides GM, Ajdari A (2002) Patterning flows using grooved surfaces. *Anal Chem* 74:5306–5312
- Sun G, Bonaccorso E, Franz V, Butt HJ (2002) Confined liquid: simultaneous observation of a molecularly layered structure and hydrodynamic slip. *J Chem Phys* 117(22):10311–10314
- Tretheway DC, Meinhart CD (2002) Apparent fluid slip at hydrophobic microchannel walls. *Phys Fluids* 14(3):L9–L12
- Ulmanella U, Ho CM (2008) Molecular effects on boundary condition in micro/nanoliquid flows. *Phys Fluids* 20(10):101512
- Urbanek W, Zemel JN, Bau HH (1993) An investigation of the temperature dependence of Poiseuille numbers in microchannel flow. *J Micromech Microeng* 3(4):206–208
- Watts P, Haswell SJ (2005) The application of microreactors for small scale organic synthesis. *Chem Eng Technol* 28(3):290–301
- Weilin Qu, Mala GM, Dongqing L (2000) Pressure-driven water flows in trapezoidal silicon microchannels. *Int J Heat Mass Transf* 43:353–364
- Wu HY, Cheng P (2003a) An experimental study of convective heat transfer in silicon microchannels with different surface conditions. *Int J Heat Mass Transf* 46(14):2547–2556
- Wu HY, Cheng P (2003b) Friction factors in smooth trapezoidal silicon microchannels with different aspect ratios. *Int J Heat Mass Transf* 46(14):2519–2525
- Xiong R (2011) Fluid flow in trapezoidal silicon microchannels with 3D random rough bottoms. *J Fluids Eng* 133(3):031102
- Xiong R, Chung JN (2010) Investigation of laminar flow in microtubes with random rough surfaces. *Microfluid Nanofluid* 8(1):11–20
- Yakovleva J, Davidsson R, Lobanova A, Bengtsson M, Eremin S, Laurell T, Emnéus J (2002) Microfluidic enzyme immunoassay using silicon microchip with immobilized antibodies and chemiluminescence detection. *Anal Chem* 74(13):2994–3004
- Zhang H, Lian L, Fu X, Zhu Z (2013) Microfluidic beads-based immunosensor for sensitive detection of cancer biomarker proteins using multi-enzyme-nanoparticle amplification and quantum dot labels. *Biosens Bioelectron* 42:23–30
- Zhou G, Yao SC (2011) Effect of surface roughness on laminar liquid flow in micro-channels. *Appl Therm Eng* 31:228–234
- Zimmermann M, Delamarque E, Wolf M, Hunziker P (2005) Modeling and optimization of high-sensitivity, low-volume microfluidic-based surface immunoassays. *Biomed Microdevices* 7(2):99–110